STATIC AEROELASTIC RESPONSE OF A ROTOR BLADE UNDER INTERNAL AXIAL LOADING

R. P. Dibble, B. K. Woods, B. Titurus

Department of Aerospace Engineering, Queen's Building, University Walk, Clifton, BS8 1TR, England

ABSTRACT

Variable speed rotors have the potential to significantly improve the performance of modern rotorcraft if the associated resonance complications can be overcome. One proposed method for resonance avoidance is to employ compressive longitudinal loads to alter the rotor's dynamic properties. This method has been shown to successfully influence a blade's dynamic properties but the following research investigates the static aeroelastic behavior of the blade under longitudinal loading.

A finite element beam model is used to investigate different methods to represent the tendon loads and determine the impact they would have on the blade's static behavior. The study demonstrates that the method for modelling tendon load is highly influential. Based on this study, the most representative and practically realisable loading model is selected to be used in further aeroelastic analysis.

A loosely coupled aeroelastic beam model is then used to represent a blade with tendon loading. The rotor was trimmed for hover and not loaded beyond its buckling load. This model demonstrates that the out-of-plane and torsional deformation, conditions for vertical trim and required power are negligibly changed in response to the considered tendon loads. These results suggest that it is possible to control the blade dynamic properties without significantly affecting the rotor performance.

1 INTRODUCTION

The rotary wing sector strives towards developing aircraft with ever increasing speed, range and endurance. However, the concepts being investigated and employed to achieve these improvements, such as variable speed rotors [1, 2] and non-uniform blade planforms, are becoming increasingly elaborate and unconventional. These concepts can achieve the desired performance improvements but they often lead to significant dynamic complications [3]. Therefore, the ability to predictably control a blade's dynamic properties is important to the success of future high-performance rotorcraft. Embedded dampers [4] were explored as a method to control transient loads in variable speed rotors. Designing for stiff, light blades [2] with high natural frequencies is another strategy for avoiding resonance in variable speed rotors.

Centrifugal forces within a rotating rotor blade contribute to the restoring forces created when the blade is perturbed from equilibrium. The increase in restoring force increases the effective stiffness and it is therefore known as 'centrifugal stiffening' [5]. The use of compressive longitudinal preloading to control dynamic properties of helicopter tail booms has been studied [6] but the use of controlled tendons to alter a blade's dynamic behaviour mid-flight is a novel area of research. In previous work [7], it was proposed that the application of a longitudinal tendon load to a rotor blade would reduce the amount of centrifugal stiffening; therefore, reducing the blade's natural frequencies. It has been demonstrated, experimentally and computationally, that natural frequency reductions of 10% of the rotor frequency can be achieved. This method could allow for variable speed rotorcraft to operate over a wider range of rotor speeds by prescribing a reduction of the blade's frequencies to avoid harmful conditions.

The effects of this method on the blade's static behaviour must be carefully evaluated. Any potentially detrimental influence of the tendon loading on the blade's static strength, stability and aerodynamic performance must be understood. Bbenefits sought through variable rotor speeds must not be outweighed by performance reductions elsewhere. The following research utilises coupled aeroelastic modelling to analyse the static aeroelastic response of a blade under longitudinal loading.

This paper initially introduces the studied blade-like structure and the different idealisations of the applied longitudinal load, herein referred to as a tendon load. Then, the static and aeroelastic models of a rotating blade in hover conditions are described and analysed.

2 MODELLING

To represent a rotor blade in hover, a set of one-dimensional rotating beam models is used. The first uses prescribed aerodynamic loads to assess the different tendon loading configurations whilst the second incorporates loosely coupled aero-structural effects for more realistic loading configuration. These models shall provide insight into the effect of the longitudinal loading on the blade's structural and aerodynamic performance as well as highlight increased sensitivities to the method of providing such loading.

Coupled in-plane, out-of-plane and torsional motions are considered in this work to ensure that all relevant shape and loading changes are captured. The subsequent beam models are designed to incorporate the effects of the centrifugal, aerodynamic and prescribed tendon loadings. Cantilevered boundary conditions are used to remove any influences of blade root/hub flexibility whilst geometrically nonlinear analyses ensure the results remain valid beyond small deflections.

The following sections describe the modelled structure, the different configurations considered to represent the tendon loading, and the beam models used for the static and aeroelastic analyses.

2.1 Equivalent blade

To maintain focus on the physics governing the behaviour of the blade, rather than the intricacies of modelling an exact blade cross-section, a simplified equivalent blade-like structure is considered.

The MBB Bo 105 has been widely studied [8, 9, 10] and it is used here as a reference aircraft. The cross section of the equivalent blade was created using ShapeDesigner SaaS 2013, a 2D FE solver [11]. As shown in Table 1 and Figure 1, it was designed to have similar geometric and selected cross-section properties to the MBB Bo 105. These include in-plane and out-of-plane stiffnesses and mass-shear offset. It was not possible to match all the properties; hence the equivalent blade is stiffer torsionally.

	MBB [8]	Equivalent
Twist [deg]	-8	0
Length [m]	4.91	5.00
Root cutout [m]	1.03	0
Rotor speed [rad/s]	44.5	50

Table 1: MBB and equivalent blade properties

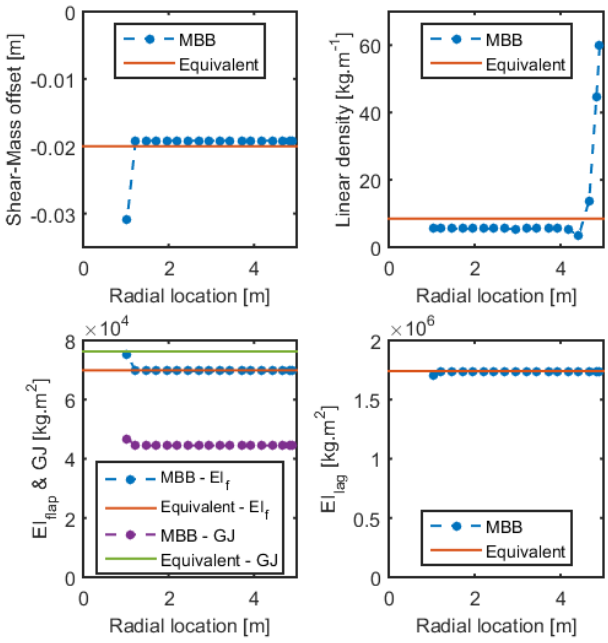

Figure 1: MBB [8] and equivalent blade distributed properties

The selected geometric attributes of the beam cross-section are summarized in Figure 2 and Table 2. The thicker leading-edge C-shaped section with a thin vertical wall is used in the equivalent blade as this provides the similar offset between the mass and shear centres. The trailing edge section is not represented as it is not a significant contributor to the cross-sectional properties.

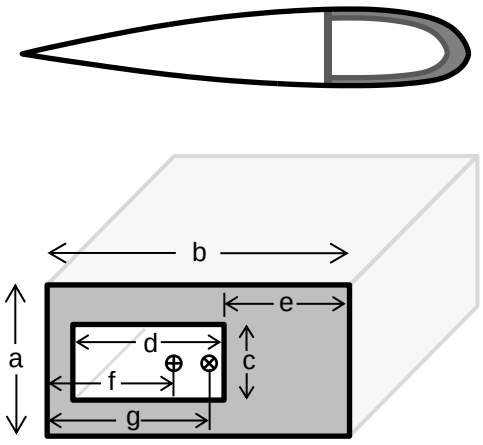

Figure 2: Example and equivalent blade cross-section

	Name	Value [m]
a	Box height	0.0332
b	Box width	0.1699
c	Cavity height	0.0032
d	Cavity width	0.1042
e	Wall thickness	0.0652
f	Shear centre	0.0615
g	Mass centre	0.0829

Table 2: Equivalent blade cross section dimensions

2.2 Tendon loading configurations

The method for applying the tendon force within the static and aeroelastic models must suitably represent the loading that would be expected from a real-world implementation. A continuous tendon running internally along the elastic axis of the undeformed blade is one likely application method. Initially, a set of four loading idealisations of the tendon effects are compared. The configuration with the best compromise between modelling realism and computational efficiency is used for the aeroelastic model.

Figure 3 shows a 2D schematic of the four loading configurations in the in-plane and out-of-plane directions of the rotating blade.

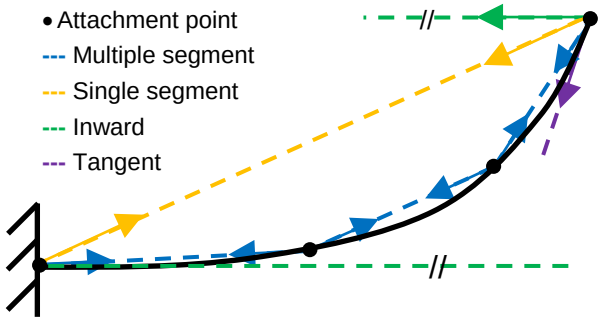

Figure 3: Loading configuration options

The arrows represent the reaction forces applied at the tendon attachment points and the dashed lines visualise the direction they are defined by.

The *multiple segment* configuration approximates a single frictionless tendon attached at the root and tip of the blade that travels through a series of evenly spaced supports. A three-segment model is shown in Figure 3 but this study uses twelve segments. The load between each of the segments is of a fixed magnitude and the deformed position of each attachment point defines the direction of the loads. The resultant load at each attachment point is projected in to the in-plane and out-of-plane directions and then applied to the models. As the direction of load vectors are dependent on the deflection of the blade, this configuration is state dependent and requires an iterative solution procedure. This configuration is the most computationally expensive but also most representative of a continuous tendon or a tendon secured at multiple ribs.

The *single segment* configuration approximates a tendon attached at the root and tip of the blade. This method is a special case of the multi segment configuration and is applied as a single load at the tip, directed towards to root of the blade. This configuration is also state dependent and an iterative solution procedure is therefore required.

The *inward* configuration applies a point load at the tip of the blade that is directed inward along the longitudinal axis of the undeformed blade. This configuration is independent of the state of the deformed blade and therefore does not require iteration.

The *tangent* configuration applies a load at the tip which is tangential to the deformed blade. This configuration will create a similar load to the multiple segment configuration at the tip but will not produce any loads at the intermediate attachment points that would be present in the multiple segment configuration.

2.3 Static analysis

To understand the implications of the different tendon loading configurations, a beam model with prescribed aerodynamic and rotational loads is developed. A Finite Element (FE) tool (Abaqus/CAE 6.14-1) is used to create the model and to perform nonlinear static and linear modal analyses.

The beam structure described in section 2.1 is meshed using 120 B31 (a 3D beam element with linear interpolation) elements. This mesh density provides convergence of the first six modes to within 0.1%. Displacements and rotations at the root are fixed to create cantilevered boundary conditions. A rotational body force is then applied to provide the centrifugal loading field that dominates a rotor blade's static and dynamic behaviour [12]. Two distributed loads are applied along the blade's elastic axis to approximate aerodynamic loading. A constant 1250N/m out-of-plane line load represents lift and a 125N/m load is applied in-plane to represent the drag the blade would produce.

The multiple and single segment configurations require an iterative procedure which is implemented using Abaqus's Python scripting environment:

1. The first iteration is completed with a 0kN tendon load.
2. The second iteration uses applied loads that are calculated based on the given tendon load and the displacements from the first iteration.
3. Subsequent iterations calculate the applied loads from the displacements of the previous two iterations and apply the mean of these two to the model.
4. Convergence is achieved when the tip deflection between the iterations changes by less than a set threshold value.

For the inward configuration, a concentrated load is applied as described in section 2.2. For the tangent configuration, a concentrated load applied at the tip uses Abaqus's follower force functionality to ensure its correct orientation.

The modal analysis is used to calculate the first six natural frequencies of the blade under rotational, aerodynamic and tendon loading. This analysis step is performed after the static loading is applied.

2.4 Aeroelastic analysis

To investigate the aerodynamic performance in hover a loosely coupled static aeroelastic model is used. A separate continuum-based model is implemented in a Matlab environment to increase the modelling flexibility and improve computational efficiency.

The structural component of the model uses the Partial Differential Equations (PDEs) derived by Hodges and Dowell [13] and solves them as a Boundary Value Problem (BVP). The PDEs are valid for long, slender beams undergoing moderate displacements. The 1D domain is divided into 12 segments to accommodate the multi-segment loading configuration.

The boundary conditions for the blade consist of a fully fixed cantilevered root, a tendon-loaded tip and intermediate continuity conditions at the segment boundaries. These continuity conditions ensure that deflections and their gradients remain continuous throughout the solution domain and that step changes in internal loads at the attachment points reflect the presence of the applied tendon loads.

The internal forces and bending moments for the boundary conditions represent the simplified formulation based on [13]. These internal loads are defined as follows

(1)
$$M_{x^+} = EAK_A{}^2(\theta' + \varphi')\left(u' + \frac{v'^2}{2} + \frac{w'^2}{2}\right) + EB_1{}^*\theta'^2\varphi' + EB_2{}^*\theta'(v''\cos\theta + w''\sin\theta) + GJ\varphi'$$

(2)
$$M_{y^+} = EI_y(v''\sin(\theta+\varphi) - w''\cos(\theta+\varphi))$$

(3)
$$M_{z^+} = EI_z(v''\cos(\theta+\varphi) + w''\sin(\theta+\varphi)) - EAe_a\left(u' + \frac{v'^2}{2} + \frac{w'^2}{2}\right) - EB_2{}^*\theta'\varphi'$$

(4)
$$V_{x^+} = EA\left(u' + \frac{v'^2}{2} + \frac{w'^2}{2} + K_A{}^2\theta'\varphi' - e_a(v''\cos(\theta+\varphi) + w''\sin(\theta+\varphi))\right)$$

(5)
$$V_y = -M'_{y^+}\sin(\theta+\varphi) - M'_z\cos(\theta+\varphi) + V_{x^+}v' + me(\Omega^2 R\cos(\theta+\varphi))$$

(6)
$$V_z = M'_{y^+}\cos(\theta+\varphi) - M'_{z^+}\sin(\theta+\varphi) + V_{x^+}w' + me(\Omega^2 R\sin(\theta+\varphi))$$

where *x*, *y* and *z* are the axial, in-plane and out-of-plane axes of the undeformed blade; [ ]$^+$ denotes the rotated axis after deformation; M_{x+}, M_{y+} and M_{z+}, are moments in the x^+, y^+ and z^+ axes, respectively; V_{x+}, V_{y+} and V_{z+}, are shear forces in the x^+, y^+ and z^+ axes, respectively; *G* and *E* are shear and Young's moduli; *J* is the torsional rigidity constant; I_y and I_z are the blade cross-section moment of inertias about the *y* and *z* axes; *u*, *v*, *w* and φ are the axial, in-plane, out-of-plane and torsional blade deformations, respectively; [ ]' is the spatial derivative with respect to x; θ is the pretwist angle; *A* is the cross sectional area; *e* and e_A are the mass centroid and tensile axis offset from the elastic axis; B_1* and B_2* are the blade section integrals [13]; K_A is the radius of gyration of blade cross section; *m* is the mass per unit length; *R* is the radius of the blade; and Ω is the rotor speed.

The attachment point equilibrium load, $\{\}_{APE,[\,]}$, is calculated to ensure the load equilibrium is maintained at each attachment point. It is calculated as the sum of the change in the internal load increment across the attachment point and the net applied tendon load.

The fully fixed root and tendon-loaded tip are implemented by enforcing the following boundary conditions at the root and tip of the blade

(7) $$u = v = v' = w = w' = \varphi = 0$$

(8) $$M_{APE,x^+} = M_{APE,y^+} = M_{APE,z^+} = V_{APE,x^+} = V_{APE,y} = V_{APE,z} = 0$$

The intermediate boundary conditions that enforce the geometric and loading continuities are defined as follows

(9) $$\Delta u = \Delta v = \Delta v' = \Delta w = \Delta w' = \Delta\varphi = 0$$

(10) $$M_{APE,x^+} = M_{APE,y^+} = M_{APE,z^+} = V_{APE,x^+} = V_{APE,y} = V_{APE,z} = 0$$

where Δ denotes the change at the boundary between the segments.

The beam structure used for this model is the same as the equivalent blade in section 2.3 with the additional inclusion of the -8° linear twist. This feature is required to obtain more realistic aerodynamic loading. Additionally, this effect increases the coupling between the in-plane and out-of-plane motions.

The aerodynamic loads are calculated using the Blade Element Momentum approach [14]. They are applied along the axis of the aerodynamic centres which is coincident with the axis of the mass centres. The blade is treated as a one-dimensional structure. At each element, the local air velocities and corresponding angles are calculated and then used to determine the aerodynamic loads. The inflow velocity is calculated iteratively to ensure that the calculated lift equates to the lift calculated using momentum theory for each element. The effective angle of attack α_e is defined as follows

(11) $$\alpha_e(r) = \theta + \varphi(r) + \beta(r) - \tan^{-1}\left(\frac{v_i}{\Omega r}\right)$$

where the in-plane velocity is defined by the radial location r and the rotor speed Ω; v_i is the inflow velocity, θ is the blade root pitch angle and φ is the torsional deformation and β is linear twist.

The distributed lift l and drag d are

(12) $$l(r) = \frac{1}{2}\rho((\Omega r)^2 + {v_i}^2)cC_l(\alpha_e)$$

(13) $$d(r) = \frac{1}{2}\rho((\Omega r)^2 + {v_i}^2)cC_d(\alpha_e)$$

where the aerodynamic coefficients (C_l, C_d) are calculated using α_e and a lookup table of experimental data for the SC1095 aerofoil over a full 360° range of angles and Mach numbers from 0 to 1 [15]. The values for air density and chord are denoted by ρ and c, respectively.

The theoretical lift [14] calculated from the momentum flow through each element of the rotor is

(14) $$l_{mom} = 2\rho dA{v_i}^2$$

where dA is the annular increment of the rotor disc area.

The PDEs [13] and boundary conditions (1)-(6) result in a static aeroelastic Boundary Value Problem. These equations are written as a series of first order PDEs in the state space form [16]. To avoid singularity in the formulation, an additional constraint, $\frac{\partial^2\varphi}{\partial x^2} = 0$, is imposed. This constraint affects cross sectional warping [13] but this is not expected to be the dominant influence in the slender beam structure considered in this study. The Boundary Value Problem in the state space form is solved using the collocation solver, *bvp4c*, implemented in *Matlab R2015a* [16].

Initially, the aerodynamic forces are calculated based on the undeformed blade shape and these forces, in turn, are used for the static shape calculation. The static shape is then used to recalculate the aerodynamic forces. The process repeats until the shape change between the consecutive iterations is less than the set threshold value of 1×10^{-6}m in displacements and 1×10^{-6}rad in torsion.

A vertical trim is required to replicate hover. This is achieved by combining the aforementioned model with a trust region algorithm [17] to calculate the blade root pitch angle that equates lift and weight to within a tolerance of 1×10^{-2} N.

The aerodynamic performance of the blade was calculated by multiplying the net torque at the rotor shaft by the rotor speed to calculate the required power for the blade.

3 CASE STUDY

3.1 Blade without tendon loads

This section analyses the baseline blade without the effects of the tendon loads. It is expected that the static shape of the blade under rotational and aerodynamic loading will significantly influence the effects of the tendon loading. Figure 4 shows the shape of the baseline blade under these rotational and aerodynamic loadings for a range of rotor speeds. Positive out-of-plane and in-plane deflection are defined as upwards and rearwards, respectively.

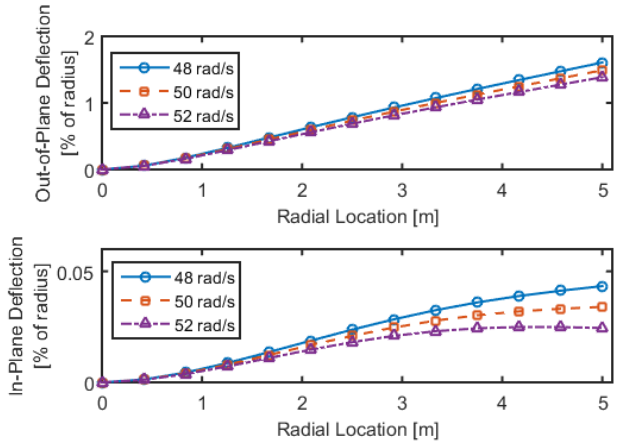

Figure 4: Deformed shape without tendon loading

The effect of rotor speed on the different directions is considerably different. The out-of-plane deflection responds classically with the reduction in centrifugal forces (rotor speed) causing a greater deflection due to the aerodynamic loads. The in-plane deflection demonstrates a similar increase in deflection with reduced rotor speeds. Additionally, the in-plane deflection also demonstrates a negative curvature. This curvature is due to the mass axis lying rearward of the elastic axis which causes a forward bending moment. As the rotor speed increases, it can be seen that the curvature of the blade increases. Overall, the relatively small deflections (<2%) indicate that the blade responses are well within the linear range of flexural deformations.

3.2 Buckling loads

Buckling is a common failure mode of axially loaded structures. Therefore, this section focuses on buckling analysis of the rotating blade with prescribed aerodynamic and tendon loads. Previous research showed that, while the natural frequencies decrease with tendon loading, their sensitivity to it increases as the buckling load is approached [7, 17]. This trait could be used for establishing the criteria for safe application of this control method.

The buckling load can be defined as the load at which the lowest eigenvalue (i.e. the square of the natural frequency) reaches zero, indicating a singular stiffness matrix [18]. The buckling load can be also defined as the load which, as approached, yields deflections that grow without limit [19]. Due to the multiple definitions, both the static deflections and eigenvalues are tracked to allow both buckling indicators to be investigated.

The statics model described in Section 2.3 is used to analyse the change in eigenvalues and deflections with increasing tendon load.

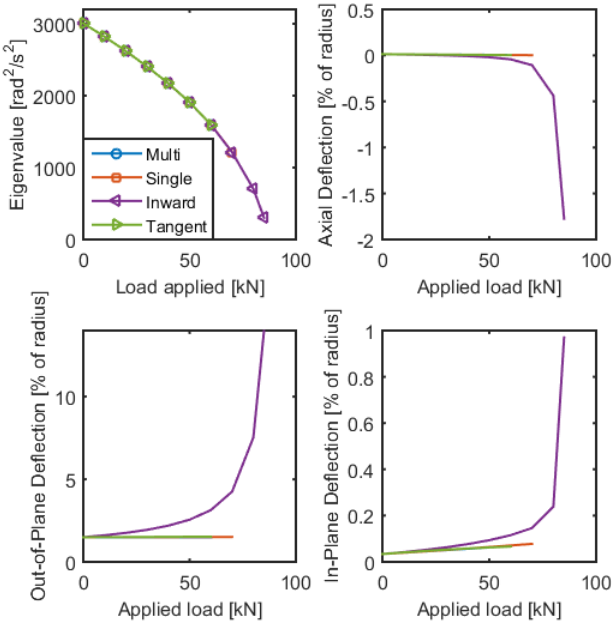

Figure 5: Buckling indicator tracking

The behaviour of the inward loading configuration in Figure 5 features the expected classical behaviour. The lowest eigenvalue decreases with the applied load whilst the sensitivity of the eigenvalue to the loading increases as the buckling load is approached. Similarly, the magnitude of the difference in deflection (from the unloaded shape described in section 3) increases, as does its sensitivity to the loading.

Despite initially similar response trends, the state dependent configurations fail to converge at higher loading values. Therefore, only the Inward configuration is used in the analysis in Figure 6.

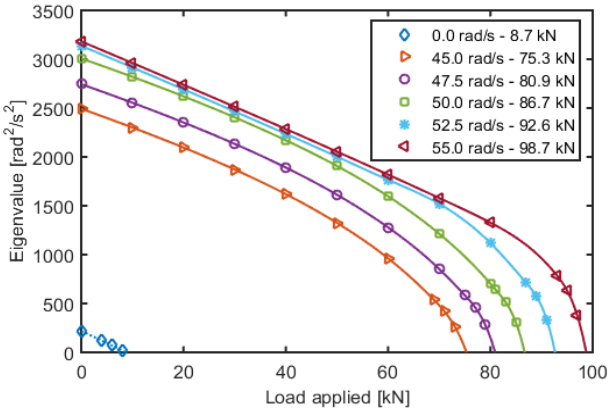

Figure 6: Rotor speed and tendon load effect on eigenvalues (no aerodynamic load for 0 rad/s)

Figure 6 shows that the eigenvalues and buckling loads are significantly larger for the higher rotor speeds. This is due to the larger centrifugal loads increasing the tension within the blade. The equation of motion for an axially and transversally loaded Euler-Bernoulli beam [5] is

$$[EIY'']'' - [TY']' - p^2 mY = F(Y) \quad (15)$$

where T is the axial load (e.g. distributed centrifugal tension) and p^2 is the eigenvalue.

Equation (15) indicates that there is an approximately linear relationship between axial load and eigenvalues. As the tendon load acts predominantly in the axial direction, it is expected that the relationship between the tendon load and blade eigenvalue will also be approximately linear. This linearity is observed at the lower tendon loads but the trend becomes increasingly nonlinear as the buckling load is approached.

To understand the proximity to the buckling, the buckling load must be determined. To estimate buckling load values, a cubic spline fit is used to extrapolate the load at which the eigenvalue equals zero. Results of this process are shown in Figure 6.

3.3 Tendon configuration selection

Out of the four configurations introduced in section 2.2, the multiple segment model represents the most realistic loading case. However, if the other configurations produce similar responses then they can be considered for use in the aeroelastic model to reduce computational cost.

The static shapes of the blade under the effects of different tendon loading configurations are compared in Figure 7. A load of 50kN is used for all the configurations to ensure they would not present any convergence failures, as observed in Figure 5.

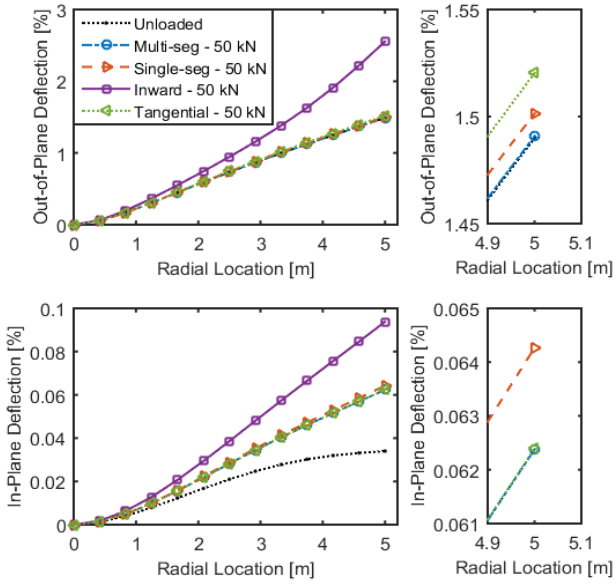

Figure 7: Static shapes for each loading configuration

Figure 7 shows that the inward configuration differs significantly from the three state dependent configurations. This figureFigure 7 also shows that the disparity between the inward configuration and the others is greatest in the out-of-plane direction.

To try to understand the cause of the differences between the configurations, the contributions to the blade root moments from the tendon loads are calculated. These moments are displayed in Figure 8 with the total moments shown in the legend. Positive moments are defined as causing positive deflections.

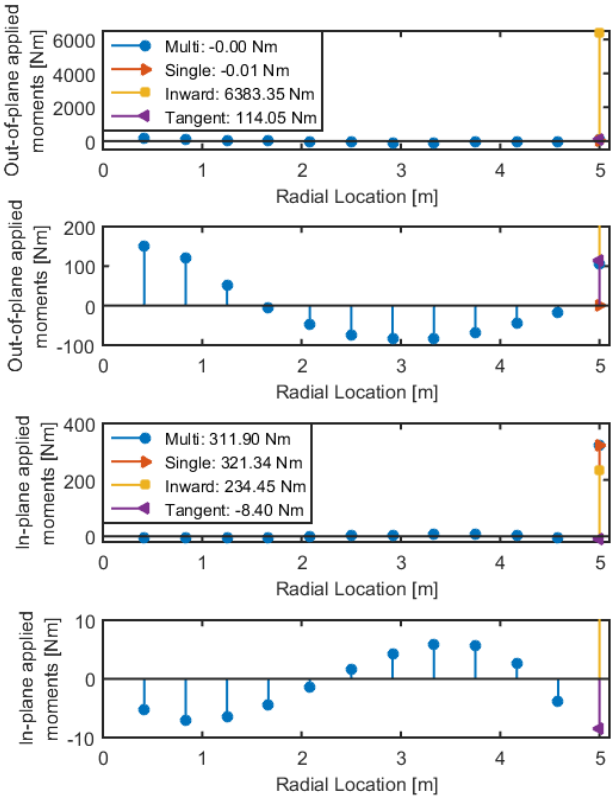

Figure 8: Root bending moment contributions loads

Figure 8 shows that the inward model creates the largest out-of-plane bending moment and hence the largest out-of-plane deflection. Due to the significant difference with the multi segment configuration in the out-of-plane deflection, the inward configuration is not considered for the aeroelastic model. The tangential model provides an almost identical change in in-plane deflection to the multi segment configuration, despite its different tendon loading profile. However, the change in out-of-plane deflection from the unloaded case is significantly greater than the multi segment model. Therefore, it is not considered for the aeroelastic model. The single segment model produces very similar total moments in both directions. It also produces similar change in in-plane deflection. However, akin to the tangential model, the response in out-of-plane deflection is not sufficiently similar to the multi segment model so it shall not be used for the aeroelastic model.

It can be concluded that none of the alternative configurations produce sufficiently similar shape changes to the multiple segment model. Therefore, despite its computational expense, this configuration is used in the following aeroelastic study.

3.4 Rotating blade in hover

To analyse the effects of tendon loads on aerodynamic performance and the aeroelastic responses, the model described in section 2.4 is used. The blade has -8º linear twist, a non-zero blade root angle to achieve hover trim and the multiple segment configuration for the tendon load.

Firstly, the static shapes of the blade under different tendon loads are compared in Figure 9. The tendon loads span from unloaded, up to near buckling to cover the full range of possible loads. Positive out-of-plane and in-plane deflection are defined as upwards and rearwards, respectively.

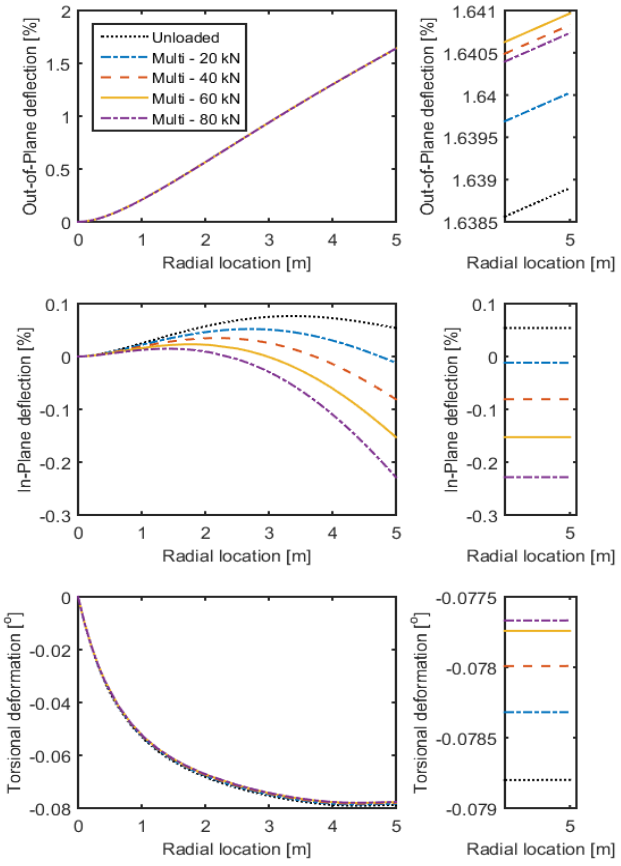

Figure 9: Comparison of aeroelastic static shapes under applied loads

Figure 9 shows that the in-plane deflections are more sensitive to tendon loading than the out-of-plane deflections. This trend is consistent with Figure 7, however the tendon loading causing a negative change in deflection is not consistent. This contradicts the idealisation that tendon loading acts as a reduction in centrifugal tension. Figure 4 shows that a reduction in centrifugal tension (rotor speed) increases in-plane and out-of-plane deflection in the positive direction. Figure 7 correlates with this idealisation as the applied load causes an increase in positive deflection. Conversely, Figure 9 shows that an increase in tendon load leads to a change of in-plane deflection in the negative direction. Torsional deformation, like out-of-plane deflection, is almost unaffected by tendon loading. Due to the lack of torsional sensitivity it is not expected that tendon loading will lead to static aeroelastic divergence.

The aerodynamic performance of the blade was calculated for a range of rotor speeds. The power and trim condition were monitored as seen in Figure 10.

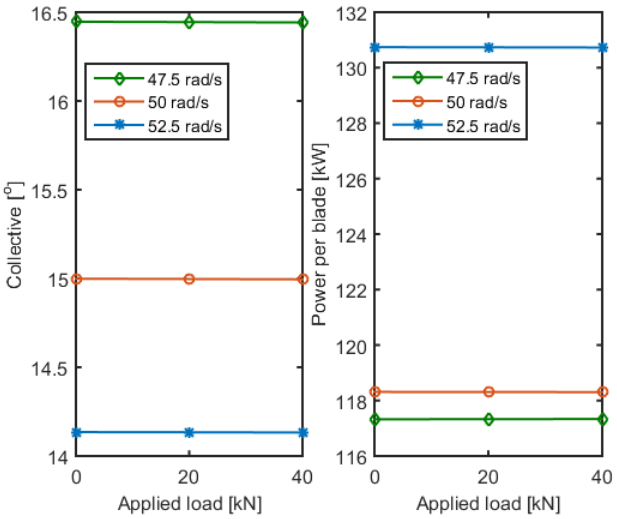

Figure 10: Blade root angle and rotor power for range of rotor speeds

Figure 10 shows that trim conditions and power vary greatly for different rotor speeds. However, due to the low sensitivity of torsional deformation to the tendon, the trim conditions and rotor power are negligibly sensitive to the tendon loading.

3.5 Modal analysis with tendon loads

The primary purpose of the applied loads is to alter the blade's natural frequencies. The model described in 2.3, using the multiple segment loading configuration, is used for modal analysis. Figure 11 shows the change in the natural frequencies with increasing tendon load, normalised against their corresponding 0kN values. It can be seen that tendon loading significantly influences the blade's natural frequencies.

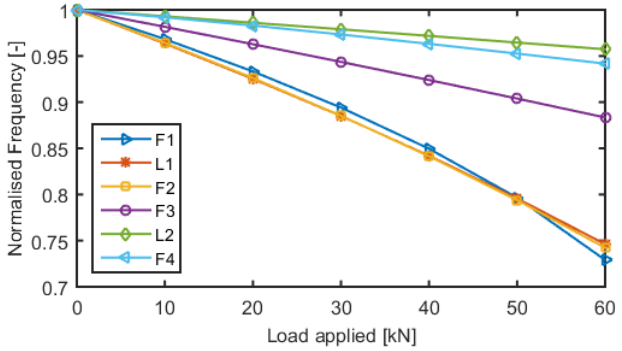

Figure 11: Change in natural frequency with applied loading

The ability to retain considerable influence over the dynamic properties of the blade corresponds well with previous research [7]. In general, the trend is for the lower frequency modes to be more sensitive to the tendon loading. In operation, the lower modes will be forced by the lower rotor harmonics which contain the most energy. Therefore, it is beneficial for these modes to be more sensitive to the tendon load.

4 CONCLUSION

The comparison of results from four different tendon loading configurations highlighted the influence and significance of the application method for the tendon loading. The single segment, inward and tangential model all produced applied load distributions and changes in responses that differ significantly from that of the multiple segment configuration. Therefore, the multiple segment configuration was used for the aeroelastic analysis. The aeroelastic model demonstrated that, for a given tendon loading configuration, the effect of coupling between the aerodynamics and the structure did not lead to a significant change in the blade static responses. Due to this, no appreciable influence on the blade trim conditions and required rotor power was observed.

It was also shown that the sensitivity of natural frequencies to tendon loading from previous work was upheld. Further research in this area will be performed to reinforce and further the understanding of the static stability characteristics and the differing effects of tendon loading on static and dynamic responses.

ACKNOWLEDGEMENTS

The author would like to thank The UK Vertical Lift Network and ESPRC for their guidance and funding, without which this research would not have been possible.

5 REFERENCES

[1] M. Allongue, H. Marze and F. Potdevin, “Quiet Helicopter 'from research to reality',” in *55th Annual AHS Forum Proceedings*, Montreal, 1999.

[2] A. E. Karem, “OPTIMUM SPEED ROTOR”. United States Patent 6,007,298, 28 December 1999.

[3] D. Han and E. Smith, “Lagwise dynamic analysis of a variable speed rotor,” *Aerospace Science and Technology,* vol. 29, no. 1, pp. 277-286, 2013.

[4] D. Han, J. Wang, E. C. Smith and G. A. Lesieutre, “Transient Loads Control of a Variable Speed Rotor During Lagwise Resonance Crossing,” *AIAA Journal,* vol. 51, no. 1, pp. 20-29, 2013.

[5] S. Newman, The Foundations of Helicopter Flight.

[6] J. D. Bois, N. Lieven and S. Adhikari, “Adaptive Passive Control of Dynamic Response through Structural Loading,” in *48th AIAA/ASME/ASCE/AHS/ASC Structures, Structural Dynamics and Materials Conference*, Honolulu, 2007.

[7] R. P. Dibble and B. Titurus, “Helicopter rotor blade modal tuning using internal preloads,” in *Proceedings of the ISMA International Conference on Noise and Vibration Engineering*, Leuven, 2016.

[8] J. A. Staley, “Validation of Rotorcraft Flight Simulation Program through Correlation with Flight Data for Soft-in-Plane Hingeless Rotors,” AMRDL, 1976.

[9] J. W. Taylor, Jane's All the World's Aircraft, Jane's Information Group, 1988.

[10] R. W. Prouty, Helicopter Performance, Stability and Control, 1986.

[11] MechaTools Technologies, “User Guide & Techniques,” 2010.

[12] K.-V. Truong, H. Yeo and R. A. Ormiston, “Structural dynamics modeling of rectangular

rotor blades," *Aerospace Science and Technology,* vol. 30, pp. 293-305, 2013.

[13] D. H. Hodges and E. H. Dowell, "Nonlinear equations of motion for the elastic bending and torsion of twisted nonuniform rotor blades," NASA Technical Note D-7818, 1974.

[14] J. G. Leishman, Principles of Helicopter Aerodynamics, 2000.

[15] J. J. Howlett, "UH-60A Black Hawk engineering simulation program. Volume 1: Mathematical model," Technical Report NASA CR 166309, 1981.

[16] L. F. Shampine, J. Kierzenka and M. Reichelt, *Solving Boundary Value Problems for Ordinary Differential Equations in MATLAB with bvp4c,* Natick, MA: The Mathworks, Inc, 2000.

[17] Y. Q. Zhang, Y. Lu, S. L. Wang and X. Liu, "Vibration and buckling of a double-beam system under compressive axial loading," *Journal of Sound and Vibration,* vol. 318, pp. 341-352, 2008.

[18] Simulia, "Abaqus Analysis User Guide," 2016.

[19] S. P. Timoshenko and J. M. Gere, Theory of Elastic Stability.